

UltrAvatar: A Realistic Animatable 3D Avatar Diffusion Model with Authenticity Guided Textures

Mingyuan Zhou^{*1}, Rakib Hyder^{*1}, Ziwei Xuan¹, Guojun Qi^{1,2}

¹OPPO US Research Center, InnoPeak Technology, Inc., USA, ²Westlake University, China

{mingyuan.zhou, rakib.hyder, ziwei.xuan}@innopeaktech.com, guojunq@gmail.com



Figure 1. **UltrAvatar**. Our method takes a text prompt or a single image as input to generate realistic animatable 3D Avatars with PBR textures, which are compatible with various rendering engines, our generation results in a wide diversity, high quality, and excellent fidelity.

Abstract

Recent advances in 3D avatar generation have gained significant attentions. These breakthroughs aim to produce more realistic animatable avatars, narrowing the gap between virtual and real-world experiences. Most of existing works employ Score Distillation Sampling (SDS) loss, combined with a differentiable renderer and text condition, to guide a diffusion model in generating 3D avatars. However, SDS often generates oversmoothed results with few facial details, thereby lacking the diversity compared with ancestral sampling. On the other hand, other works generate 3D avatar from a single image, where the challenges of unwanted lighting effects, perspective views, and inferior image quality make them difficult to reliably reconstruct the 3D face meshes with the aligned complete textures. In this paper, we propose a novel 3D avatar generation approach termed UltrAvatar with enhanced fidelity of geometry, and superior quality of physically based rendering (PBR) textures without unwanted lighting. To this end, the proposed approach presents a diffuse color extraction model and an

authenticity guided texture diffusion model. The former removes the unwanted lighting effects to reveal true diffuse colors so that the generated avatars can be rendered under various lighting conditions. The latter follows two gradient-based guidances for generating PBR textures to render diverse face-identity features and details better aligning with 3D mesh geometry. We demonstrate the effectiveness and robustness of the proposed method, outperforming the state-of-the-art methods by a large margin in the experiments.

1. Introduction

Generating 3D facial avatars is of significant interest in the communities of both computer vision and computer graphics. Recent advancements in deep learning have greatly enhanced the realism of AI-generated avatars. Although multi-view 3D reconstruction methods, such as Multi-View Stereo (MVS) [66] and Structure from Motion (SfM) [65], have facilitated avatar generation from multiple images captured at various angles, generating realistic 3D avatars from few images, like a single view taken by user or particularly generated from text prompts, proves significantly challeng-

* Equal contribution.

ing due to the limited visibility, unwanted lighting effects and inferior image quality.

Previous works have attempted to overcome these challenges by leveraging available information contained in the single view image. For example, [24, 46, 79] focused on estimating parameters of the 3D Morphable Model (3DMM) model by minimizing landmark loss and photometric loss, and other approaches train a self-supervised network to predict 3DMM parameters [20, 25, 64, 80]. These methods are sensitive to occlusions and lighting conditions, leading to susceptible 3DMM parameters or generation of poor quality textures. Moreover, many existing works [20, 25, 79, 80] rely on prefixed texture basis [31] to generate facial textures. Although these textures are often reconstructed jointly with lighting parameters, the true face colors and skin details are missing in the underlying texture basis and thus are unable to be recovered. Alternatively, other works [8, 10, 37, 73] employ neural radiance rendering field (NeRF) to generate 3D Avatar, but they are computationally demanding and not amenable to mesh-based animation of 3D avatars. They also may lack photo-realism when being rendered from previously unobserved perspectives.

Generative models [29, 30, 43, 53, 61, 75] designed for 3D avatars have shown promising to generate consistent 3D meshes and textures. However, these models do not account for unwanted lighting effects that prevent access to true face colors and could result in deteriorated diffuse textures. On the other hand, some works use the SDS loss [56, 75, 76] to train a 3D avatar by aligning the rendered view with the textures generated by a diffusion model. The SDS may lead to the oversmoothed results that lack the diversity in skin and facial details compared with the original 2D images sampled from the underlying diffusion model.

To address these challenges, we propose a novel approach to create 3D animatable avatars that are more realistic in diffuse colors and skin details. First, our approach can take either a text prompt or a single face image as input. The text prompt is fed into a generic diffusion model to create a face image, or the a single face image can also be input into our framework. It is well known that separating lighting from the captured colors in a single image is intrinsically challenging. To obtain high quality textures that are not contaminated by the unwanted lighting, our key observation is that the self-attention block in the diffusion model indeed captures the lighting effects, this enables us to reveal the true diffuse colors by proposing a diffuse color extraction (DCE) model to robustly eliminate the lighting from the texture of the input image.

In addition, we propose to train an authenticity guided texture diffusion model (AGT-DM) that are able to generate high-quality complete facial textures that align with the 3D face meshes. Two gradient guidances are presented to

enhance the resultant 3D avatars – a photometric guidance and an edge guidance that are added to classifier-free diffusion sampling process. This can improve the diversity of the generated 3D avatars with more subtle high-frequency details in their facial textures across observed and unobserved views.

The key contributions of our work are summarized below.

- We reveal the relationship between the self-attention features and the lighting effects, enabling us to propose a novel model for extracting diffuse colors by removing lighting effects in a single image. Our experiments demonstrate this is a robust and effective approach, suitable for tasks such as removing specular spotlights and shadows.
- We introduce an authenticity guided diffusion model to generate PBR textures. It can provide high-quality complete textures that well align with 3D meshes without susceptible lighting effects. The sampling process follows two gradient-based guidances to retain facial details unique to each identity, which contributes to the improved generation diversity.
- We build a novel 3D avatar generative framework UltrAvatar upon the proposed DCE model and the AGT-DM. Our experiments demonstrate high quality diverse 3D avatars with true colors and sharp details (see Fig. 1).

2. Related Work

Image-to-Avatar Generation: Initially, avatar generation was predominantly reliant on complex and costly scanning setups, limiting its scalability [7, 13, 33, 48]. This challenge has shifted towards utilizing common image inputs like a single photo [20, 25, 80] or video [16, 28, 32, 79]. Additionally, the representation of 3D head has diversified, ranging from the mesh-based parametric models [46, 79] to the fluid neural implicit functions like NeRFs [8, 37, 73]. The introduction of advanced neural networks, especially Generative Adversarial Networks (GANs) [40] have led to the embedding of 3D attributes directly into these generative models [17, 21, 52] and the use of generative model as a prior to generate 3D avatars [29, 30, 43, 44] etc. Some techniques [10, 23] also can create the riggable avatars from a single image. Nevertheless, these existing methods rely on the provided images for mesh and texture generation, often encounter errors in mesh creation and issues with diffuse texture generation due to the lighting like specular highlights and shadows on the images. Our proposed method adeptly addresses and mitigates these challenges, ensuring more consistent and accurate results.

Text-to-3D Generation: Text-to-3D generation is a popular research topic that builds on the success of text-to-image models [51, 58–60]. DreamFusion [56],

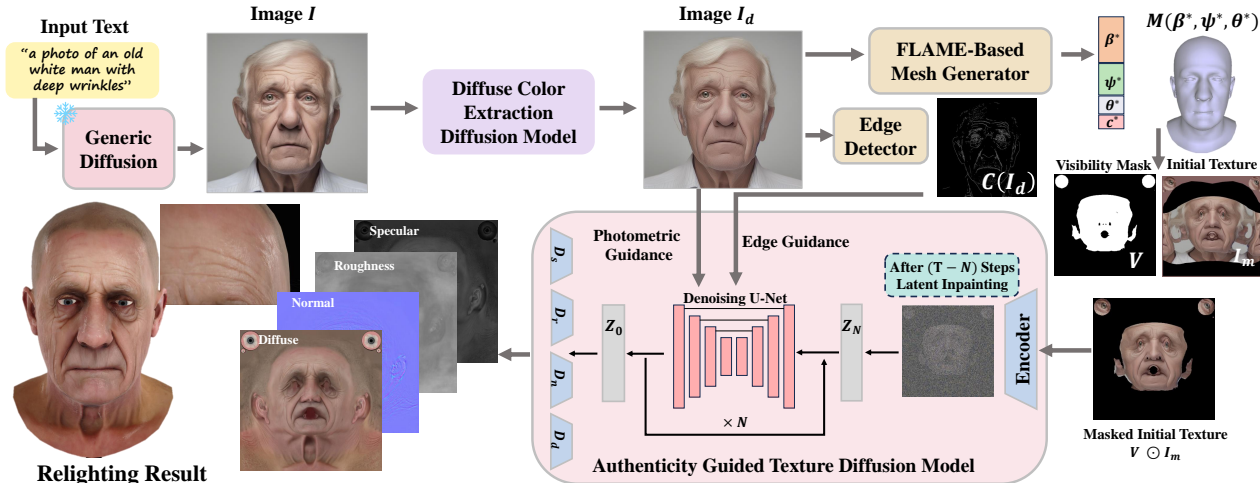


Figure 2. **The Overview of UltraAvatar.** First, we feed a text prompt into a generic diffusion model (SDXL [55]) to produce a face image. Alternatively, the face image can also be directly input into our framework. Second, our DCE model takes the face image to extract its diffuse colors I_d by eliminating lighting. The I_d is then passed to the mesh generator and the edge detector to generate the 3D mesh, camera parameters and the edge image. With these predicted parameters, the initial texture and the corresponding visibility mask can be created by texture mapping. Lastly, we input the masked initial texture into our AGT-DM to generate the PBR textures. A relighting result using the generated mesh and PBR textures is shown here.

Magic3D [47], Latent-NeRF [49], AvatarCLIP [36], Clip-Face [9], Rodin [70], DreamFace [76] etc., uses the text prompt to guide the 3D generation. Most of these approaches use SDS loss to maintain consistency between the images generated by the diffusion model and 3D object. However, SDS loss significantly limits the diversity of generation. Our approach upholds the powerful image generation capabilities from diffusion models trained on large scale data, facilitating diversity. Simultaneously, it ensures a high degree of fidelity between the textual prompts and the resulting avatars without depending on SDS loss.

Guided Diffusion Model: A salient feature of diffusion models lies in their adaptability post-training, achieved by guiding the sampling process to tailor outputs. The concept of guided diffusion has been extensively explored in a range of applications, encompassing tasks like image super-resolution [18, 27, 63], colorization [19, 62], deblurring [18, 71], and style-transfer [26, 41, 42]. Recent studies have revealed that the diffusion U-Net’s intermediate features are rich in information about the structure and content of generated images [12, 34, 42, 57, 69]. We discover that the attention features can represent lighting in the image and propose a method to extract the diffuse colors from a given image. Additionally, we incorporated two guidances to ensure the authenticity and realism of the generated avatars.

3. The Method

An overview of our framework is illustrated in Fig. 2. We take a face image as input or use the text prompt to generate

a view I of the avatar with a diffusion model. Then, we introduce a DCE model to recover diffuse colors by eliminating unwanted lighting from the generated image. This process is key to generating high quality textures without being deteriorated by lighting effects such as specularity and shadows. This also ensures the generated avatars can be properly rendered under new lighting conditions. We apply a 3D face model (e.g., a 3DMM model) to generate the mesh aligned with the resultant diffuse face image. Finally, we train an AGT-DM with several decoders to generate PBR textures, including diffuse colors, normal, specular, and roughness textures. This complete set of PBR textures can well align with the 3D mesh, as well as preserve the face details unique to individual identity.

3.1. Preliminaries

Diffusion models learn to adeptly transform random noise with condition y into a clear image by progressively removing the noise. These models are based on two essential processes. The forward process initiates with a clear image x_0 and incrementally introduces noise, culminating in a noisy image x_T , and the backward process works to gradually remove the noise from x_T , restoring the clear image x_0 . The stable diffusion (SD) model [55, 60] operates within the latent space $z = E(x)$ by encoding the image x to a latent representation. The final denoised RGB image is obtained by decoding the latent image through $x_0 = D(z_0)$. To carry out the sequential denoising, the network ϵ_θ is rigorously trained to predict noise at each time step t by following the objective function:

$$\min_{\theta} \mathbb{E}_{z \sim E(x), t, \epsilon \sim \mathcal{N}(0,1)} \|\epsilon - \epsilon_{\theta}(z_t, t, \tau(y))\|_2^2. \quad (1)$$

where the $\tau(\cdot)$ is the conditioning encoder for an input condition y , such as a text embedding, z_t represents the noisy latent sample at the time step t . The noise prediction model in SD is based on the U-Net architecture, where each layer consists of a residual block, a self-attention block, and a cross-attention block, as depicted in Fig. 4. At a denoising step t , the features ϕ_t^{l-1} from the previous $(l-1)$ -th layer are relayed to the residual block to produce the res-features f_t^l . Within the self-attention block, the combined features $(\phi_t^{l-1} + f_t^l)$ through the residual connection are projected to the query features q_t^l , key features k_t^l and value features v_t^l . The above res-features f_t^l contributes to the content of the generated image and the attention features hold substantial information that contributes to the overall structure layout, which are normally used in image editing [34, 42, 57, 69].

Diffusion models possess the pivotal feature of employing guidance to influence the reverse process for generating conditional samples. Typically, classifier guidance can be applied to the score-based models by utilizing a distinct classifier. Ho *et al.* [35] introduce the classifier-free guidance technique, blending both conditioned noise prediction $\epsilon_{\theta}(z_t, t, \tau(y))$ and unconditioned noise prediction $\epsilon_{\theta}(z_t, t, \emptyset)$, to extrapolate one from another,

$$\tilde{\epsilon}_{\theta}(z_t, t, \tau(y)) = \omega \epsilon_{\theta}(z_t, t, \tau(y)) + (1 - \omega) \epsilon_{\theta}(z_t, t, \emptyset). \quad (2)$$

where \emptyset is the embedding of a null text and ω is the guidance scale.

3.2. Diffuse Color Extraction via Diffusion Features

Our approach creates a 3D avatar from a face image I that is either provided by a user or generated by a diffusion model [55, 60] from a text prompt. To unify the treatment of those two cases, the DDIM inversion [22, 68] with non-textual condition is applied to the image that results in a latent noise z_T^I at time step T from which the original image I is then reconstructed through the backward process. This gives rise to a set of features from the diffusion model.

The given image I , no matter user-provided or SD-generated, typically contains shadows, specular highlights, and lighting effects that are hard to eliminate. To render a reliable and animatable 3D avatar, it usually requires a diffuse texture map with these lighting effects removed from the image, which is a challenging task. For this, we make a key observation that reveals the relation between the self-attention features and the lighting effects in the image, and introduce a DCE model to eliminate the lighting.

First, we note that the features f_t^l in each layer contain the RGB details as discussed in [67, 69]. The self-attention

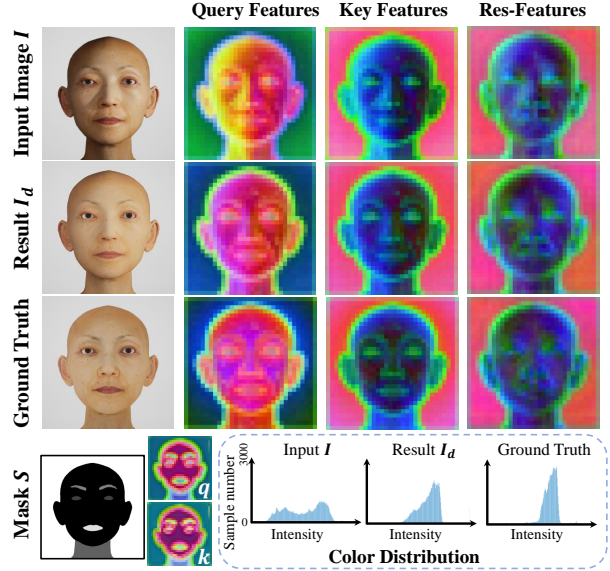


Figure 3. **Features Visualization.** We render a high-quality data with PBR textures under a complex lighting condition to image I , and also render its corresponding ground truth diffuse color image. We input the I to our DCE model to produce result I_d . The S is the semantic mask. We apply DDIM inversion and sampling on these images and extract the features. To visualize the features, we apply PCA on the extracted features to check the first three principal components. The attention features and res-features shown here are all from the 8-th layer at upsampling layers in the U-Net at time step 101. From the extracted query and key features of I , we can clearly visualize the lighting. The colors and extracted query and key features of the result I_d closely match those from the ground truth image, which demonstrates our method effectively removes the lighting. All res-features do not present too much lighting. We also show the color distributions of these three images, illustrating that the result I_d can eliminate shadows and specular points, making its distribution similar to the ground truth.

features q_t^l and k_t^l reflect the image layout, with similar regions exhibiting similar values. Beyond this, our finding is that the variations in these self-attention features q_t^l and k_t^l indeed reflect the variations caused by the lighting effects such as shading, shadows, and specular highlights within a semantic region. This is illustrated in Fig. 3. This is not hard to understand. Consider a pixel on the face image, its query features ought to align with the key features from the same facial part so that its color can be retrieved from the relevant pixels. With the lighting added to the image, the query features must vary in the same way as the variation caused by the lighting effects. In this way, the lighted colors could be correctly retrieved corresponding to the lighting pattern – shadows contribute to the colors of nearby shadowed pixels, while highlights contribute to the colors of nearby high-lighted ones.

To eliminate lighting effects, one just needs to remove the variation in the self-attention (query and key) features

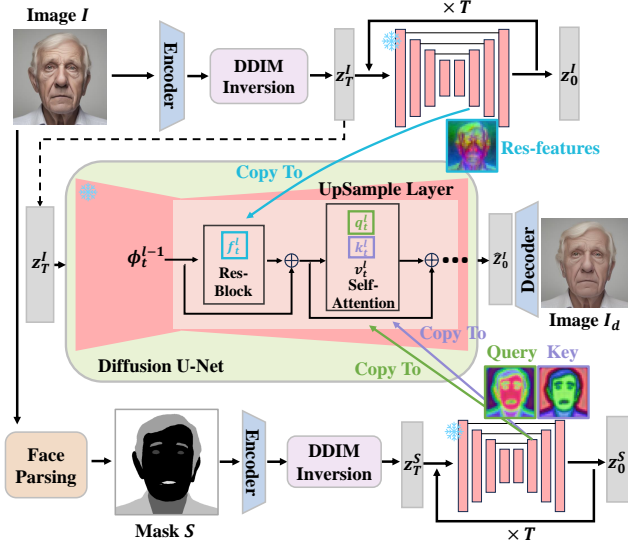


Figure 4. **DCE Model**. The input image I is fed to the face parsing model to create the semantic mask S . We apply DDIM inversion on the I and S to get initial noise z_T^I and z_T^S , then we progressively denoise the z_T^I and z_T^S to extract and preserve the res-features and attention features separately. Lastly, we progressively denoise the z_T^I one more time, copying the res-features and attention features from storage at certain layers (as discussed in Sec. 4) during sampling to produce \hat{z}_0^I , the final result I_d will be generated from decoding the \hat{z}_0^I .

while still keeping these features aligned with the semantic structure. Fig. 4 summarizes the idea. Specifically, first we choose a face parsing model to generate a semantic mask S for the image I . The semantic mask meets the above two requirements since it perfectly aligns with the semantic structure by design and has no variation within a semantic region. Then we apply the DDIM inversion to S resulting in a latent noise z_T^S at time step T , and obtain the self-attention features of S via the backward process starting from z_T^S for further replacing q_i^l and k_i^l of the original I . Since the semantic mask has uniform values within a semantic region, the resultant self-attention features are hypothesized to contain no lighting effects (see Fig. 3), while the face details are still kept in the features f_i^l of the original image I . Thus, by replacing the query and key features q_i^l and k_i^l with those from the semantic mask in the self-attention block, we are able to eliminate the lighting effects from I and keep its diffuse colors through the backward process starting from the latent noise z_T^I used for generating I .

This approach can be applied to eliminate lighting effects from more generic images other than face images, and we show more results in the Appendix.

3.3. 3D Avatar Mesh Generation

We employ the FLAME [46] model as our geometry representation of 3D avatars. FLAME is a 3D head template

model, which is trained from over 33,000 scans. It is characterized by the parameters for identity shape β , facial expression ψ and pose parameters θ . With these parameters. FLAME generates a mesh $M(\beta, \psi, \theta)$ consisting 5023 vertices and 9976 faces, including head, neck, and eyeballs meshes. We adopt MICA [80] for estimating shape code β^* of the FLAME model from the diffuse image I_d , which excels in accurately estimating the neutral face shape and is robust to expression, illumination, and camera changes. We additionally apply EMOCA [20] to obtain the expression code ψ^* , pose parameters θ^* and camera parameters c^* , which is employed for subsequent 3D animation/driving applications. Note that we do not use the color texture generated by the EMOCA combining the FLAME texture basis. It cannot accurately present the true face color, lacks skin details and contains no PBR details, such as diffuse colors, normal maps, specularity, and roughness textures, which can be derived below with our AGT-DM.

3.4. Authenticity Guided Texture Diffusion Model

Given the current estimated mesh $M(\beta^*, \psi^*, \theta^*)$, camera parameters c^* and the lighting-free face image I_d , one can do the texture mapping of the latter onto the mesh, and then project the obtained mesh texture to an initial texture UV map I_m . Since I_d is only a single view of the face, the resultant I_m is an incomplete UV texture map of diffuse colors, and we use V to denote its visible mask in the UV coordinates. The UV texture map may also not perfectly align with the mesh due to the errors in the estimated face pose, expression and camera pose by EMOCA.

To address the above challenges, we train an AGT-DM that can 1) inpaint the partially observed texture UV map I_m to the full UV coordinates, and 2) improve the alignment between the texture map and the UV coordinates. Moreover, the model can output more PBR details beyond the diffuse color textures, including normal, specular and roughness maps from the given I_m and V . We will enhance the output PBR results with two guidance signals based on the photometric and edge details, so that the identity and more facial features, such as subtle wrinkles and pores, can be recovered from the AGT-DM.

To this end, we use the online 3DScan dataset [1] that consists of 3D face scans alongside multiple types of PBR texture maps (in 4K and 8K) including diffuse colors, normal maps, specularity and roughness textures on the entire high-quality meshes of 3D scans. We process this dataset (details in the Appendix) into a training dataset and train an inpainting SD model with them, the U-net of the original SD is finetuned over the groundtruth diffuse UV maps from the dataset. To generate PBR textures, the SD encoder is frozen and the SD decoder is copied and finetuned over the dataset for each type of PBR texture, except that the PBR decoder D_d for diffuse texture directly inherits

from the original SD decoder. Then we can use the fine-tuned SD model to inpaint the masked diffuse color map $V \odot I_m$ alongside the other PBR textures. Because the training dataset have ideally aligned meshes and texture details, the resultant inpainting diffusion model can improve the alignment between the output PBR textures and meshes, as well as facial details. Denoising the noisy masked texture latent Z_N following latent inpainting, more accurate alignment can be generated between textures and meshes since the denoising could corrupt the misalignments in I_m and allow the inpainting diffusion model to correct them through diffusion sampling.

To further enhance the PBR textures with more facial details, we employ two energy functions to guide the sampling process of the inpainting diffusion model. The first is the photometric guidance G_P with the following energy function,

$$G_P = \omega_{photo} \|V_d \odot (R(M(\beta^*, \psi^*, \theta^*), D_d(z_t), c^*) - I_d)\|_2^2 + \omega_{lpips} L_{lpips}(V_d \odot (R(M(\beta^*, \psi^*, \theta^*), D_d(z_t), c^*)), V_d \odot I_d) \quad (3)$$

where V_d is the mask over the visible part of rendered face, as shown in Fig. 6, and the $R(\cdot)$ is a differential renderer of the avatar face based on the current estimate of the mesh M , the diffuse color texture map $D_d(z_t)$ at a diffusion time step t , the $L_{lpips}(\cdot)$ is the perceptual loss function (LPIPS [77]). The minimization of this photometric energy will align the rendered image with the original image.

The second is the edge guidance with the following edge energy function,

$$G_E = \|V_d \odot (C(R(M(\beta^*, \psi^*, \theta^*), D_d(z_t), c^*)) - C(I_d))\|_2^2 \quad (4)$$

where $C(\cdot)$ is the canny edge detection function [15]. While the edges contain high-frequency details, as shown in Fig. 2, this guidance will help retain the facial details such as wrinkles, freckles, pores, moles and scars in the image I_d , making the generated avatars look more realistic with high fidelity.

We integrate the two guidances through the gradients of their energy functions into the sampling of classifier-free guidance below,

$$\tilde{c}_\theta(z_t, t, \tau(y)) = \omega_{\epsilon_\theta}(z_t, t, \tau(y)) + (1 - \omega)\epsilon_\theta(z_t, t, \emptyset) + \omega_p \nabla_{z_t} G_P + \omega_e \nabla_{z_t} G_E. \quad (5)$$

We demonstrate the effectiveness in Fig 6.

4. Experiments

4.1. Setup and Baselines

Experimental Setup. We used SDXL[55] as our text-to-image generation model. We used pretrained BiSeNet [4, 74] for generating face parsing mask, S . In our DCE

module, we use the standard SD-2.1 base model and apply the DDIM sampling with 20 time steps. We preserve the res-features from 4th to 11th upsampling layers in the U-net extracted from the I , and inject into the DDIM sampling of I the query and key features from the 4th to 9th upsampling layers extracted from S . We choose not to inject query and key features from all layers because we find injecting them to the last few layers sometimes slightly would change the identity.

For our AGT-DM, we finetune the U-Net from SD-2.1-base model on our annotated 3DScan store dataset to generate diffuse color texture map. We attach ‘‘A UV map of’’ to the text prompt during finetuning to generate FLAME UV maps. We train three decoders to output normal, specular and roughness maps. More training details are presented in the Appendix.

In the AGT-DM, we use $T = 200$, $N = 90$, $\omega = 7.5$, $\omega_p = 0.1$, $\omega_{photo} = 0.4$, $\omega_{lpips} = 0.6$ and $\omega_e = 0.05$. In the initial $T - N$ denoising steps, our approach adopts a latent space inpainting technique akin to the method described in [11], utilizing a visibility mask. During the final N steps, we apply the proposed photometric and edge guidances to rectify any misalignments and ensure a coherent integration between the observed and unobserved regions of the face. After the inference, we pass the resultant latent code to normal, specular and roughness decoders to obtain the corresponding PBR texture maps. We then pass the texture to a pretrained Stable Diffusion super-resolution network [60] to get 2K resolution texture.

Baselines. We show comparisons against different state-of-the-art approaches for text-to-avatar generation (Latent3d [14], CLIPMatrix [38], Text2Mesh[50], CLIPFace[9], DreamFace[76]) and image-to-avatar generation (FlameTex[24], PanoHead [8]). Details about the comparisons are included in the Appendix.

4.2. Results and Discussion

We demonstrate our text/image generated realistic avatars in Fig. 1 and 5. Note that, we do not have those images in the training data for our AGT-DM. Generated results demonstrate rich textures maintaining fidelity with the given text prompt/image. Furthermore, due to our DCE model and AGT-DM’s capabilities to extract diffuse color texture and PBR details, we can correctly render relighted avatars from any lighting condition. Since, AGT-DM enforces consistency across the observed and unobserved region, our rendered avatars look equally realistic from different angles without any visible artifacts.

Performance Analysis. For comparison, we randomly select 40 text prompts, ensuring a comprehensive representation across various age groups, ethnicities and genders, as well as including a range of celebrities. For Dream-

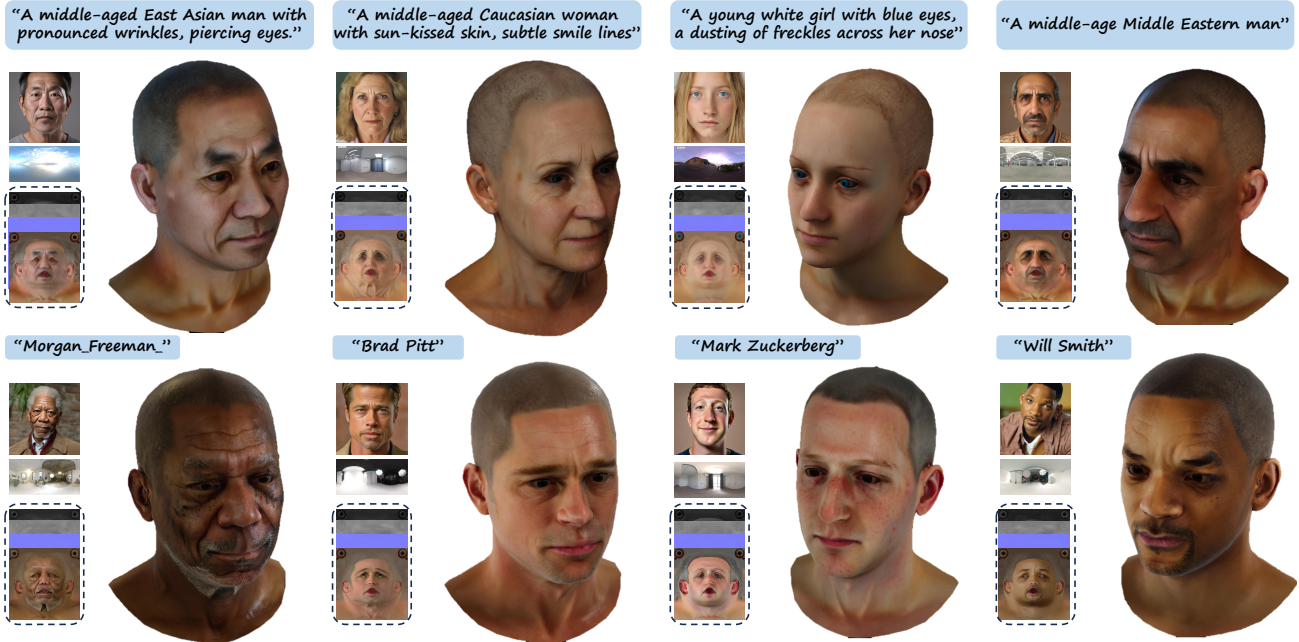


Figure 5. **Results of generating random identities and celebrities.** We input the text prompts into the generic SDXL to create 2D face images. Our results showcase the reconstructed high-quality PBR textures which are also well-aligned with the meshes, exhibit high fidelity, and maintain the identity and facial details. To illustrate the quality of our generation, we relight each 3D avatar under various environment maps.

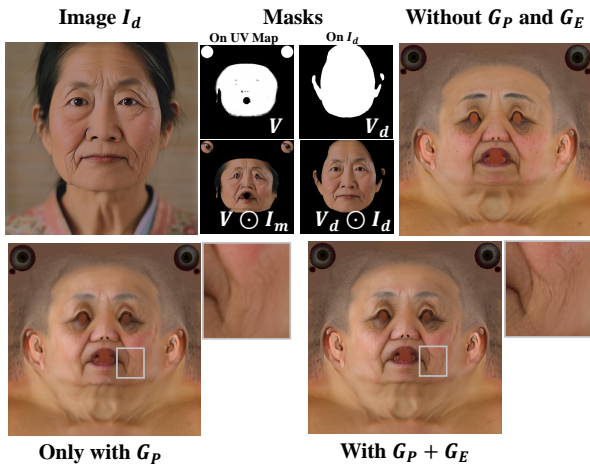


Figure 6. **Analysis of the guidances in the AGT-DM.** Three PBR textures generation scenarios from image I_d by our AGT-DM are shown: one without G_P and G_E , one only with G_P , and another with both G_P and G_E . It clearly demonstrates that the identity and facial details are effectively maintained through these two guidances.

Face and UltrAvatar, we render the generated meshes from 50 different angles under 5 different lighting conditions. For PanoHead, we provide 200 images generated by SDXL using the same 40 text prompts. UltrAvatar can generate high-quality facial asset from text prompt within 2 minutes (compared to 5 minutes for DreamFace) on a single Nvidia

A6000 GPU.

We evaluate the perceptual quality of the rendered images using standard generative model metrics FID and KID. Similar to CLIPFace, we evaluate both of these metrics with respect to masked FFHQ images [39] (without background, eyes and mouth interior) as ground truth. For text-to-avatar generation, we additionally calculate CLIP score to measure similarity between text prompts and rendered images. We report the average score from two different CLIP variants, ‘ViT-B/16’ and ‘ViT-L/14’.

Among the text-to-avatar generation approaches in Table 1, DreamFace performs very well on maintaining similarity between text and generated avatars. However, the generated avatars by DreamFace lack realism and diversity. Our proposed UltrAvatar performs significantly better than DreamFace in terms of perceptual quality (more results are shown in the Appendix). Furthermore, in Fig. 7, we demonstrate that DreamFace fails to generate avatars from challenging prompts (e.g. big nose, uncommon celebrities). It is important to note that the results from DreamFace represent its best outputs from multiple runs. Our UltrAvatar also outperforms other text-to-avatar approaches in terms of perceptual quality and CLIP score, as reported in Table 1. In the task of image-to-avatar generation, PanoHead achieves impressive performance in rendering front views. However, the effectiveness of PanoHead is heavily dependent on the accuracy of their pre-processing steps, which occasionally

Method	FID ↓	KID ↓	CLIP Score ↑
DreamFace [76]	76.70	0.061	0.291 ± 0.020
ClipFace* [9]	80.34	0.032	0.251 ± 0.059
Latent3d*[14]	205.27	0.260	0.227 ± 0.041
ClipMatrix*[38]	198.34	0.180	0.243 ± 0.049
Text2Mesh*[50]	219.59	0.185	0.264 ± 0.044
FlameTex*[24]	88.95	0.053	-
PanoHead [8]	48.64	0.039	-
UtrAvatar (Ours)	45.50	0.029	0.301 ± 0.023

Table 1. Comparison of methods based on FID, KID, and CLIP Score metrics, * results are from CLIPFace.



Figure 7. **Comparison to DreamFace.** Our results achieve better alignment with the text prompt than DreamFace, especially for extreme prompts.

fail to provide precise estimation. Furthermore, the NeRF-based PanoHead approach is limited in relighting. Considering the multi-view rendering capabilities, UtrAvatar outperforms PanoHead in image-to-avatar task as shown in Table 1.

In addition, we automate text-to-avatar performance assessment utilizing GPT-4V(ision) [5, 6]. GPT-4V is recognized for its human-like evaluation capabilities in vision-language tasks [72, 78]. We evaluate models on a 5-point Likert scale. The criteria for assessment include photo-realism, artifact minimization, skin texture quality, textual prompt alignment, and the overall focus and sharpness of the image. As illustrated in Fig. 8, UtrAvatar demonstrates superior capabilities in generating lifelike human faces. It not only significantly reduces artifacts and enhances sharpness and focus compared to DreamFace and PanoHead but also maintains a high level of photo-realism and fidelity in text-prompt alignment.

4.3. Ablation Studies.

In Fig. 6, we illustrate the impact of different guidances on the AGT-DM performance. The photometric guidance enforces the similarity between the generated texture and the source image. Additionally, the edge guidance enhances the details in the generated color texture.

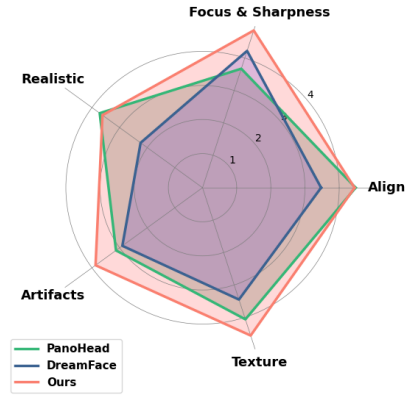


Figure 8. **Qualitative evaluation by GPT-4V.** Our framework has overall better performance.

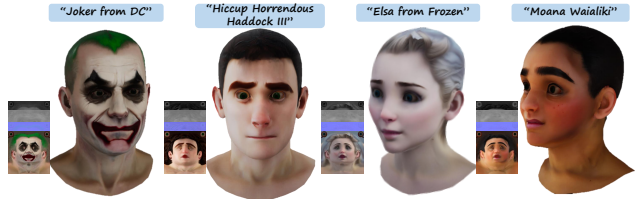


Figure 9. **Results of out-of-domain avatar generation.** Our framework has capability to generate out-of-distribution animation characters or non-human avatars.

Out-of-domain Generation. UtrAvatar can generate avatars from the image/prompt of animation characters, comic characters and other non-human characters. We have shown some results in Fig. 9.

Animation and Editing Since our generated avatars are mesh-based models, we can animate our generated avatars by changing the expressions and poses. We can also perform some texture editing using the text prompt in the AGT-DM. We have included the animation and editing results in the Appendix.

5. Conclusion

We introduced a novel approach to 3D avatar generation from either a text prompt or a single image. At the core of our method is the DCE Model designed to eliminate unwanted lighting effects from a source image, as well as a texture generation model guided by photometric and edge signals to retain the avatar’s PBR details. Compared with the other SOTA approaches, we demonstrate our method can generate 3D avatars that display heightened realistic, higher quality, superior fidelity and more extensive diversity.

References

- [1] 3DScan store. <https://www.3dscanstore.com/>. 5, 12
- [2] Wrap4d. <https://www.russian3dscanner.com/wrap4d/>. 12
- [3] Hyperhuman. <https://hyperhuman.deemos.com/>. 12
- [4] Using modified BiSeNet for face parsing in PyTorch. <https://github.com/zllrunning/face-parsing.PyTorch>. 6
- [5] ChatGPT can now see, hear, and speak. <https://openai.com/blog/chatgpt-can-now-see-hear-and-speak>, 2023. 8, 12
- [6] GPT-4V(ision) system card. https://cdn.openai.com/papers/GPTV_System_Card.pdf, 2023. 8, 12
- [7] Oleg Alexander, Mike Rogers, William Lambeth, Jen-Yuan Chiang, Wan-Chun Ma, Chuan-Chang Wang, and Paul Debevec. The Digital Emily Project: Achieving a Photorealistic Digital Actor. *IEEE Computer Graphics and Applications*, 30(4):20–31, 2010. 2
- [8] Sizhe An, Hongyi Xu, Yichun Shi, Guoxian Song, Umit Y Ogras, and Linjie Luo. PanoHead: Geometry-Aware 3D Full-Head Synthesis in 360°. In *CVPR*, pages 20950–20959, 2023. 2, 6, 8, 12
- [9] Shivangi Aneja, Justus Thies, Angela Dai, and Matthias Nießner. ClipFace: Text-guided Editing of Textured 3D Morphable Models. In *ACM SIGGRAPH 2023 Conference Proceedings*, pages 1–11, 2023. 3, 6, 8, 12
- [10] ShahRukh Athar, Zexiang Xu, Kalyan Sunkavalli, Eli Shechtman, and Zhixin Shu. RigNeRF: Fully Controllable Neural 3D Portraits. In *CVPR*, pages 20364–20373, 2022. 2
- [11] Omri Avrahami, Ohad Fried, and Dani Lischinski. Blended Latent Diffusion. *ACM TOG*, 42(4):1–11, 2023. 6, 12
- [12] Omri Avrahami, Thomas Hayes, Oran Gafni, Sonal Gupta, Yaniv Taigman, Devi Parikh, Dani Lischinski, Ohad Fried, and Xi Yin. SpaText: Spatio-Textual Representation for Controllable Image Generation. In *CVPR*, pages 18370–18380, 2023. 3
- [13] George Borshukov and John P Lewis. Realistic Human Face Rendering for “The Matrix Reloaded”. In *ACM Siggraph 2005 Courses*, pages 13–es. 2005. 2
- [14] Zehranaz Canfes, M Furkan Atasoy, Alara Dirik, and Pinar Yanardag. Text and Image Guided 3D Avatar Generation and Manipulation. In *CVPR*, pages 4421–4431, 2023. 6, 8, 12
- [15] John Canny. A Computational Approach to Edge Detection. *IEEE TPAMI*, (6):679–698, 1986. 6
- [16] Chen Cao, Tomas Simon, Jin Kyu Kim, Gabe Schwartz, Michael Zollhoefer, Shun-Suke Saito, Stephen Lombardi, Shih-En Wei, Danielle Belko, Shoou-I Yu, et al. Authentic volumetric avatars from a phone scan. *ACM TOG*, 41(4):1–19, 2022. 2
- [17] Eric R Chan, Connor Z Lin, Matthew A Chan, Koki Nagano, Boxiao Pan, Shalini De Mello, Orazio Gallo, Leonidas J Guibas, Jonathan Tremblay, Sameh Khamis, et al. Efficient Geometry-aware 3D Generative Adversarial Networks. In *CVPR*, pages 16123–16133, 2022. 2
- [18] Hyungjin Chung, Jeongsol Kim, Michael Thompson McCann, Marc Louis Klasky, and Jong Chul Ye. Diffusion Posterior Sampling for General Noisy Inverse Problems. In *ICLR*, 2022. 3
- [19] Hyungjin Chung, Byeongsu Sim, Dohoon Ryu, and Jong Chul Ye. Improving Diffusion Models for Inverse Problems using Manifold Constraints. *NeurIPS*, 35:25683–25696, 2022. 3
- [20] Radek Daněček, Michael J Black, and Timo Bolkart. EMOCA: Emotion Driven Monocular Face Capture and Animation. In *CVPR*, pages 20311–20322, 2022. 2, 5
- [21] Yu Deng, Jiaolong Yang, Jianfeng Xiang, and Xin Tong. GRAM: Generative Radiance Manifolds for 3D-Aware Image Generation. In *CVPR*, pages 10673–10683, 2022. 2
- [22] Prafulla Dhariwal and Alexander Nichol. Diffusion Models Beat GANs on Image Synthesis. *NeurIPS*, 34:8780–8794, 2021. 4
- [23] Zheng Ding, Xuaner Zhang, Zhihao Xia, Lars Jebe, Zhuowen Tu, and Xiuming Zhang. DiffusionRig: Learning Personalized Priors for Facial Appearance Editing. In *CVPR*, pages 12736–12746, 2023. 2
- [24] Haven Feng. Photometric FLAME fitting. https://github.com/HavenFeng/photometric_optimization, 2019. 2, 6, 8, 12
- [25] Yao Feng, Haiwen Feng, Michael J Black, and Timo Bolkart. Learning an Animatable Detailed 3D Face Model from In-The-Wild Images. *ACM TOG*, 40(4):1–13, 2021. 2
- [26] Rinon Gal, Yuval Alaluf, Yuval Atzmon, Or Patashnik, Amit Haim Bermano, Gal Chechik, and Daniel Cohen-or. An Image is Worth One Word: Personalizing Text-to-Image Generation using Textual Inversion. In *ICLR*, 2022. 3
- [27] Sicheng Gao, Xuhui Liu, Bohan Zeng, Sheng Xu, Yanjing Li, Xiaoyan Luo, Jianzhuang Liu, Xiantong Zhen, and Baochang Zhang. Implicit Diffusion Models for Continuous Super-Resolution. In *CVPR*, pages 10021–10030, 2023. 3
- [28] Xuan Gao, Chenglai Zhong, Jun Xiang, Yang Hong, Yudong Guo, and Juyong Zhang. Reconstructing Personalized Semantic Facial NeRF Models from Monocular Video. *ACM TOG*, 41(6):1–12, 2022. 2
- [29] Baris Gecer, Stylianos Ploumpis, Irene Kotsia, and Stefanos Zafeiriou. GANFIT: Generative Adversarial Network Fitting for High Fidelity 3D Face Reconstruction. In *CVPR*, pages 1155–1164, 2019. 2
- [30] Baris Gecer, Alexandros Lattas, Stylianos Ploumpis, Jiankang Deng, Athanasios Papaioannou, Stylianos Moschoglou, and Stefanos Zafeiriou. Synthesizing Coupled 3D Face Modalities by Trunk-Branch Generative Adversarial Networks. In *ECCV*, pages 415–433. Springer, 2020. 2
- [31] Thomas Gerig, Andreas Morel-Forster, Clemens Blumer, Bernhard Egger, Marcel Luthi, Sandro Schönborn, and Thomas Vetter. Morphable Face Models - An Open Framework. In *2018 13th IEEE International Conference on Automatic Face & Gesture Recognition (FG 2018)*, pages 75–82. IEEE, 2018. 2
- [32] Philip-William Grassal, Malte Prinzler, Titus Leistner, Carsten Rother, Matthias Nießner, and Justus Thies. Neural Head Avatars from Monocular RGB Videos. In *CVPR*, pages 18653–18664, 2022. 2

- [33] Kaiwen Guo, Peter Lincoln, Philip Davidson, Jay Busch, Xueming Yu, Matt Whalen, Geoff Harvey, Sergio Orts-Escolano, Rohit Pandey, Jason Dourgarian, et al. The relightables: Volumetric performance capture of humans with realistic relighting. *ACM TOG*, 38(6):1–19, 2019. [2](#)
- [34] Amir Hertz, Ron Mokady, Jay Tenenbaum, Kfir Aberman, Yael Pritch, and Daniel Cohen-Or. Prompt-to-Prompt Image Editing with Cross-Attention Control. In *ICLR*, 2022. [3](#), [4](#)
- [35] Jonathan Ho and Tim Salimans. Classifier-Free Diffusion Guidance. In *NeurIPS 2021 Workshop on Deep Generative Models and Downstream Applications*, 2021. [4](#)
- [36] Fangzhou Hong, Mingyuan Zhang, Liang Pan, Zhongang Cai, Lei Yang, and Ziwei Liu. AvatarCLIP: Zero-Shot Text-Driven Generation and Animation of 3D Avatars. *ACM TOG*, 41(4):1–19, 2022. [3](#)
- [37] Yang Hong, Bo Peng, Haiyao Xiao, Ligang Liu, and Juyong Zhang. HeadNeRF: A Real-time NeRF-based Parametric Head Model. In *CVPR*, pages 20374–20384, 2022. [2](#)
- [38] Nikolay Jetchev. ClipMatrix: Text-controlled Creation of 3D Textured Meshes. *arXiv preprint arXiv:2109.12922*, 2021. [6](#), [8](#), [12](#)
- [39] Tero Karras, Samuli Laine, and Timo Aila. A Style-Based Generator Architecture for Generative Adversarial Networks. In *CVPR*, pages 4401–4410, 2019. [7](#)
- [40] Tero Karras, Samuli Laine, Miika Aittala, Janne Hellsten, Jaakko Lehtinen, and Timo Aila. Analyzing and Improving the Image Quality of StyleGAN. In *CVPR*, pages 8110–8119, 2020. [2](#)
- [41] Nupur Kumari, Bingliang Zhang, Richard Zhang, Eli Shechtman, and Jun-Yan Zhu. Multi-concept customization of text-to-image diffusion. In *CVPR*, pages 1931–1941, 2023. [3](#)
- [42] Gihyun Kwon and Jong Chul Ye. Diffusion-based Image Translation using Disentangled Style and Content Representation. In *ICLR*, 2022. [3](#), [4](#)
- [43] Alexandros Lattas, Stylianos Moschoglou, Baris Gecer, Stylianos Ploumpis, Vasileios Triantafyllou, Abhijeet Ghosh, and Stefanos Zafeiriou. AvatarMe: Realistically Renderable 3D Facial Reconstruction “in-the-wild”. In *CVPR*, pages 760–769, 2020. [2](#)
- [44] Alexandros Lattas, Stylianos Moschoglou, Stylianos Ploumpis, Baris Gecer, Jiankang Deng, and Stefanos Zafeiriou. FitMe: Deep Photorealistic 3D Morphable Model Avatars. In *CVPR*, pages 8629–8640, 2023. [2](#)
- [45] Junnan Li, Dongxu Li, Silvio Savarese, and Steven Hoi. BLIP-2: Bootstrapping Language-Image Pre-training with Frozen Image Encoders and Large Language Models. 2023. [12](#)
- [46] Tianye Li, Timo Bolkart, Michael J Black, Hao Li, and Javier Romero. Learning a model of facial shape and expression from 4D scans. *ACM TOG*, 36(6), 2017. [2](#), [5](#)
- [47] Chen-Hsuan Lin, Jun Gao, Luming Tang, Towaki Takikawa, Xiaohui Zeng, Xun Huang, Karsten Kreis, Sanja Fidler, Ming-Yu Liu, and Tsung-Yi Lin. Magic3D: High-Resolution Text-to-3D Content Creation. In *CVPR*, pages 300–309, 2023. [3](#)
- [48] Stephen Lombardi, Jason Saragih, Tomas Simon, and Yaser Sheikh. Deep Appearance Models for Face Rendering. *ACM TOG*, 37(4):1–13, 2018. [2](#)
- [49] Gal Metzer, Elad Richardson, Or Patashnik, Raja Giryes, and Daniel Cohen-Or. Latent-NeRF for Shape-Guided Generation of 3D Shapes and Textures. In *CVPR*, pages 12663–12673, 2023. [3](#)
- [50] Oscar Michel, Roi Bar-On, Richard Liu, Sagie Benaim, and Rana Hanocka. Text2Mesh: Text-Driven Neural Stylization for Meshes. In *CVPR*, pages 13492–13502, 2022. [6](#), [8](#), [12](#)
- [51] Alexander Quinn Nichol, Prafulla Dhariwal, Aditya Ramesh, Pranav Shyam, Pamela Mishkin, Bob McGrew, Ilya Sutskever, and Mark Chen. GLIDE: Towards Photorealistic Image Generation and Editing with Text-Guided Diffusion Models. In *Int. Conf. Machine Learn.*, pages 16784–16804. PMLR, 2022. [2](#)
- [52] Roy Or-El, Xuan Luo, Mengyi Shan, Eli Shechtman, Jeong Joon Park, and Ira Kemelmacher-Shlizerman. StyleSDF: High-Resolution 3D-Consistent Image and Geometry Generation. In *CVPR*, pages 13503–13513, 2022. [2](#)
- [53] Foivos Paraperas Papantoniou, Alexandros Lattas, Stylianos Moschoglou, and Stefanos Zafeiriou. Relightify: Relightable 3d faces from a single image via diffusion models. *arXiv preprint arXiv:2305.06077*, 2023. [2](#)
- [54] Pascal Paysan, Reinhard Knothe, Brian Amberg, Sami Romdhani, and Thomas Vetter. A 3d face model for pose and illumination invariant face recognition. In *2009 sixth IEEE international conference on advanced video and signal based surveillance*, pages 296–301. Ieee, 2009. [12](#)
- [55] Dustin Podell, Zion English, Kyle Lacey, Andreas Blattmann, Tim Dockhorn, Jonas Müller, Joe Penna, and Robin Rombach. SDXL: Improving Latent Diffusion Models for High-Resolution Image Synthesis. *arXiv preprint arXiv:2307.01952*, 2023. [3](#), [4](#), [6](#)
- [56] Ben Poole, Ajay Jain, Jonathan T Barron, and Ben Mildenhall. DreamFusion: Text-to-3D using 2D Diffusion. In *ICLR*, 2022. [2](#)
- [57] Konpat Preechakul, Nattanat Chatthee, Suttisak Wizatwongsa, and Supasorn Suwajanakorn. Diffusion Autoencoders: Toward a Meaningful and Decodable Representation. In *CVPR*, pages 10619–10629, 2022. [3](#), [4](#)
- [58] Aditya Ramesh, Mikhail Pavlov, Gabriel Goh, Scott Gray, Chelsea Voss, Alec Radford, Mark Chen, and Ilya Sutskever. Zero-Shot Text-to-Image Generation. In *Int. Conf. Machine Learn.*, pages 8821–8831. PMLR, 2021. [2](#)
- [59] Aditya Ramesh, Prafulla Dhariwal, Alex Nichol, Casey Chu, and Mark Chen. Hierarchical Text-Conditional Image Generation with CLIP Latents. *arXiv preprint arXiv:2204.06125*, 1(2):3, 2022.
- [60] Robin Rombach, Andreas Blattmann, Dominik Lorenz, Patrick Esser, and Björn Ommer. High-Resolution Image Synthesis with Latent Diffusion Models. In *CVPR*, pages 10684–10695, 2022. [2](#), [3](#), [4](#), [6](#)
- [61] Will Rowan, Patrik Huber, Nick Pears, and Andrew Keeling. Text2Face: A Multi-Modal 3D Face Model. *arXiv preprint arXiv:2303.02688*, 2023. [2](#)

- [62] Chitwan Saharia, William Chan, Huiwen Chang, Chris Lee, Jonathan Ho, Tim Salimans, David Fleet, and Mohammad Norouzi. Palette: Image-to-Image Diffusion Models. In *ACM SIGGRAPH 2022 Conference Proceedings*, pages 1–10, 2022. 3
- [63] Chitwan Saharia, Jonathan Ho, William Chan, Tim Salimans, David J Fleet, and Mohammad Norouzi. Image Super-Resolution via Iterative Refinement. *IEEE TPAMI*, 45(4): 4713–4726, 2022. 3
- [64] Soubhik Sanyal, Timo Bolkart, Haiwen Feng, and Michael J Black. Learning to Regress 3D Face Shape and Expression from an Image without 3D Supervision. In *CVPR*, pages 7763–7772, 2019. 2
- [65] Johannes L Schonberger and Jan-Michael Frahm. Structure-from-Motion Revisited. In *CVPR*, pages 4104–4113, 2016. 1
- [66] Steven M Seitz, Brian Curless, James Diebel, Daniel Scharstein, and Richard Szeliski. A Comparison and Evaluation of Multi-View Stereo Reconstruction Algorithms. In *CVPR*, pages 519–528. IEEE, 2006. 1
- [67] Chenyang Si, Ziqi Huang, Yuming Jiang, and Ziwei Liu. FreeU: Free Lunch in Diffusion U-Net. *arXiv preprint arXiv:2309.11497*, 2023. 4
- [68] Jiaming Song, Chenlin Meng, and Stefano Ermon. Denoising diffusion implicit models. In *ICLR*, 2021. 4
- [69] Narek Tumanyan, Michal Geyer, Shai Bagon, and Tali Dekel. Plug-and-Play Diffusion Features for Text-Driven Image-to-Image Translation. In *CVPR*, pages 1921–1930, 2023. 3, 4
- [70] Tengfei Wang, Bo Zhang, Ting Zhang, Shuyang Gu, Jianmin Bao, Tadas Baltrusaitis, Jingjing Shen, Dong Chen, Fang Wen, Qifeng Chen, et al. Rodin: A Generative Model for Sculpting 3D Digital Avatars Using Diffusion. In *CVPR*, pages 4563–4573, 2023. 3
- [71] Jay Whang, Mauricio Delbracio, Hossein Talebi, Chitwan Saharia, Alexandros G Dimakis, and Peyman Milanfar. Deblurring via Stochastic Refinement. In *CVPR*, pages 16293–16303, 2022. 3
- [72] Zhengyuan Yang, Linjie Li, Kevin Lin, Jianfeng Wang, Chung-Ching Lin, Zicheng Liu, and Lijuan Wang. The Dawn of LMMs: Preliminary Explorations with GPT-4V(ision), 2023. 8, 12
- [73] Yu Yin, Kamran Ghasedi, HsiangTao Wu, Jiaolong Yang, Xin Tong, and Yun Fu. NeRFInventor: High Fidelity NeRF-GAN Inversion for Single-shot Real Image Animation. In *CVPR*, pages 8539–8548, 2023. 2
- [74] Changqian Yu, Jingbo Wang, Chao Peng, Changxin Gao, Gang Yu, and Nong Sang. BiSeNet: Bilateral Segmentation Network for Real-time Semantic Segmentation. In *ECCV*, pages 325–341, 2018. 6
- [75] Hao Zhang, Yao Feng, Peter Kulits, Yandong Wen, Justus Thies, and Michael J Black. Text-Guided Generation and Editing of Compositional 3D Avatars. *arXiv preprint arXiv:2309.07125*, 2023. 2
- [76] Longwen Zhang, Qiwei Qiu, Hongyang Lin, Qixuan Zhang, Cheng Shi, Wei Yang, Ye Shi, Sibe Yang, Lan Xu, and Jingyi Yu. DreamFace: Progressive Generation of Animatable 3D Faces under Text Guidance. *ACM TOG*, 42(4), 2023. 2, 3, 6, 8, 12
- [77] Richard Zhang, Phillip Isola, Alexei A Efros, Eli Shechtman, and Oliver Wang. The Unreasonable Effectiveness of Deep Features as a Perceptual Metric. In *Proceedings of the IEEE conference on computer vision and pattern recognition*, pages 586–595, 2018. 6
- [78] Xinlu Zhang, Yujie Lu, Weizhi Wang, An Yan, Jun Yan, Lianke Qin, Heng Wang, Xifeng Yan, William Yang Wang, and Linda Ruth Petzold. GPT-4V(ision) as a Generalist Evaluator for Vision-Language Tasks, 2023. 8, 12
- [79] Yufeng Zheng, Victoria Fernández Abrevaya, Marcel C Bühler, Xu Chen, Michael J Black, and Otmar Hilliges. I M Avatar: Implicit Morphable Head Avatars from Videos. In *CVPR*, pages 13545–13555, 2022. 2
- [80] Wojciech Zielonka, Timo Bolkart, and Justus Thies. Towards Metrical Reconstruction of Human Faces. In *ECCV*, pages 250–269. Springer, 2022. 2, 5

Appendix

A. Experimental Setup

A.1. Dataset

We use the 3DScan dataset comprising 188 super-high quality commercial data samples from the [1], encompassing a diverse array of skin colors, skin tones, genders, ages, and ethnicities. For each identity, the data includes high-quality 3D head and eyeball meshes, along with diffuse, normal, roughness, and specular textures in high resolution (4K and 8K). Notably, the textures provided are identical to ground truth and the diffuse map doesn't contain any lighting effects. We register all 3D meshes from the dataset to the FLAME mesh format and align all of the texture maps with FLAME UV mapping through commercial Wrap4D [2]. We annotate the dataset based on individual identity attributes: skin color, gender, ethnicity, and age.

A.2. PBR Texture Decoders Training

We use the dataset to train separate decoders for normal, specular and roughness textures estimation. We directly apply variational autoencoder (VAE) from SD-2.1-base model for diffuse texture, we freeze the encoder, take the diffuse texture as input and finetune 3 separate decoders to generate other maps over the dataset. We optimize the decoders by minimizing the loss function $L_D = \|D_{\{n,s,r\}}(E(I_m)) - I_{\{n,s,r\}}\|_2^2 + \lambda L_{lips}(D_{\{n,s,r\}}(E(I_m)), I_{\{n,s,r\}})$, where D_n , D_s and D_r are normal, specular and roughness decoders, $E(\cdot)$ is the SD-2.1-base encoder, I_n , I_s , I_r and I_m correspond to normal, specular, roughness and diffuse texture maps respectively.

A.3. Inpainting

We perform latent inpainting in the first $(T - N)$ steps of the diffusion denoising process. We downsample the visibility mask V to the latent visibility mask V^* and encode I_m into the latent code $z^m = E(I_m)$. Similar to [11], at each denoising step, we apply inpainting by updating $z_t^* = V^* \odot (z^m + \epsilon_t) + (1 - V^*) \odot z_t$, where z_t is the denoised latent and ϵ_t is the scheduled noise for time-step t .

When the image is used as the input, we use BLIP-2 [45] to generate caption which would eventually be fed to our AGT-DM. For neutral face mesh generation, we set expression and pose parameters to zero.

B. Evaluation Details

B.1. Baselines

Latent3d [14] uses text or image-based prompts to change the shape and texture of a 3D model. It combines CLIP and a 3D GAN with a differentiable renderer to adjust the input latent codes for specific attribute manipulation while keeping the other attributes unchanged.

CLIPMatrix [38] leverages CLIP text embeddings to create high-resolution, articulated 3D meshes controlled by text prompts.

Text2Mesh[50] stylizes 3D meshes based on text prompts, using a neural style field network and CLIP model for style editing. It does not rely on pre-trained models or specialized datasets.

CLIPFace[9] uses text to control 3D faces' expressions and appearance. It combines 3D models and a generative model to make expressive, textured, and articulated faces with adversarial training and differentiable rendering.

DreamFace [76] is a progressive text-guided method designed to generate personalized, animatable 3D face assets compatible with CG pipelines, enabling users to customize faces with specific shapes, textures, and detailed animations. Since DreamFace does not have any implementation publicly available, we used their website UI [3] to generate and download meshes with all PBR textures.

FlameTex[24] is a PCA-based texturing model tailored for the FLAME model, developed using 1500 randomly selected images from the FFHQ dataset and the base texture is from the Basel Face Model [54].

PanoHead [8] makes view-consistent 360° images of full human heads from unstructured images. It uses novel 3D GAN training and feature entanglement resolution techniques to create avatars from single images.

B.2. Qualitative Comparison

We present eight samples respectively generated from our UltraAvatar, DreamFace and PanoHead under one lighting condition in our quantitative comparison experiment for qualitative visualization, in Fig. 10. There are corresponding eight prompts which are from our 40 prompts used in comparison experiment. We use Unreal Engine for rendering. We display results from three viewpoints (frontal view, left view at -45 degree angle, right view at 45 degree angle) for each method. Additionally, the middle images from PanoHead results, generated from the input prompts, are their and our inputs. In the comparison, UltraAvatar delivers higher quality results and achieves more accurate alignment between the input texts and the generated avatars. PanoHead provides satisfactory results but in a low resolution, there are many artifacts along the edges and boundaries when zoomed, moreover, it is incapable of producing animatable avatars.

B.3. Evaluation from the GPT4-V

The recently released GPT-4V(sion) [5, 6] is recognized as an effective evaluation tool with outstanding human-alignment for images [72, 78]. We leverage GPT-4V to qualitatively rate the rendered images of generated avatars. We request that GPT-4V conduct assessments based on the five criteria: photo-realism, artifact minimization, skin tex-

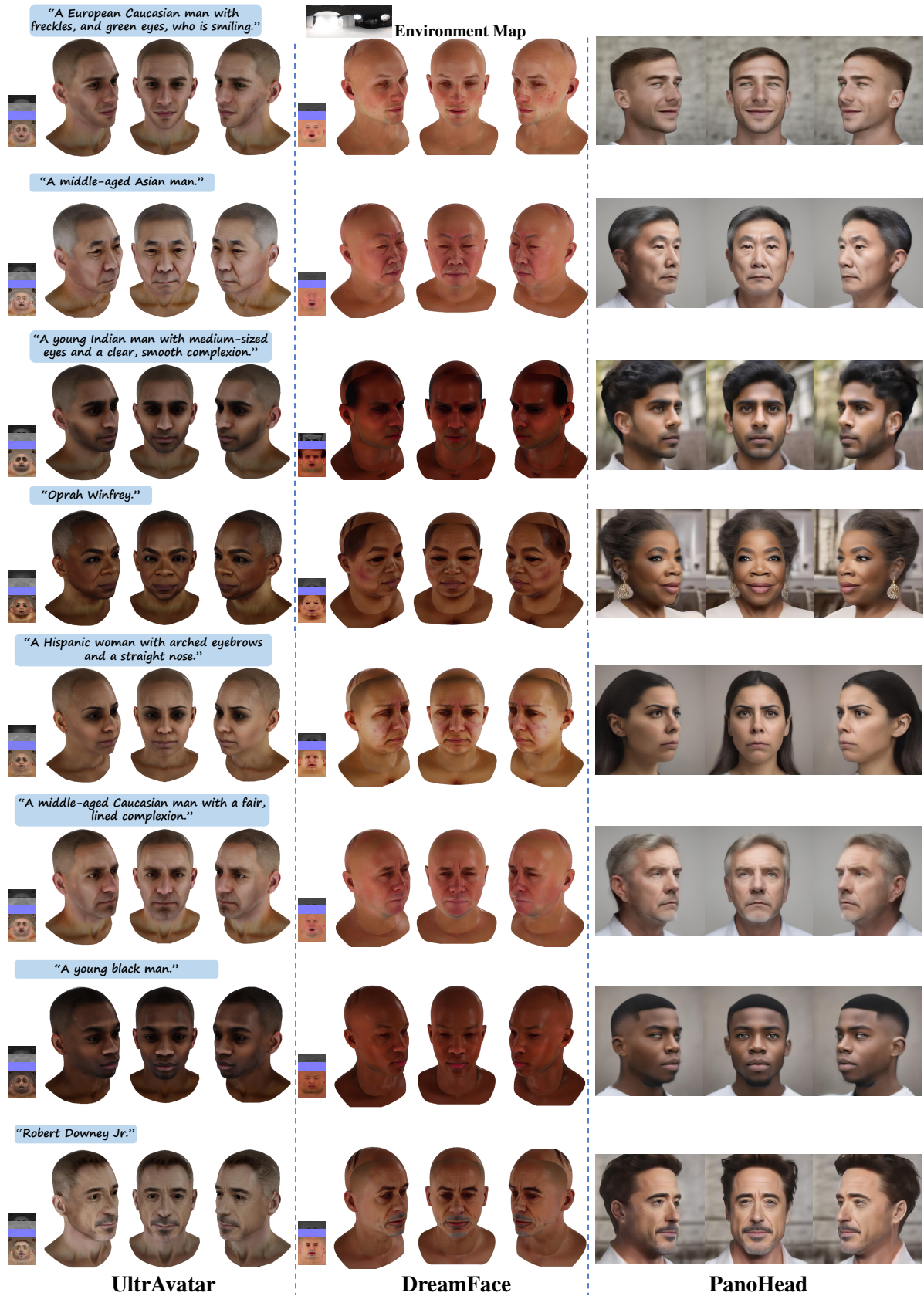


Figure 10. **Qualitative Comparison.** We show some results from our quantitative comparison experiment involving DreamFace and PanoHead. UltrAvatar produces higher quality, greater diversity, better fidelity results, clearly outperforms the state-of-the-art methods.



Figure 11. **Texture Editing Results.** Our AGT-DM has capability to execute texture editing, editing results are shown here, including changing eye and hair colors, aging effects, and adding tattoos.

ture quality, textual prompt alignment, and the overall focus and sharpness of the images. We define the situations in which a high or a low score will be assigned, prompt the GPT-4V API with the following instructions and draw the comparison figure using five-point Likert scale based on the average score for each criterion.

```
Please act as a professional photography critic.
You are provided a picture of a human face.
Please rate it from five dimensions.
1. Reality. Please score this picture for how
much it looks like a real person. The score
range is 1-5. A score of 1 means the poorest
reality and the picture is assumed to be fake
, while a score of 5 means the highest
reality and the picture captures a real
person.
2. Alignment. Please score how much this picture
reflects the theme {image_prompt}. The score
range is 1-5. A score of 1 means the provided
picture does not reflect the theme at all,
while a score of 5 means the picture
perfectly reflects the theme.
3. Focus and Sharpness. Please score how good
this portrait picture from the perspective of
focus and sharpness. The score range is 1-5.
A score of 1 means the picture has a soft
focus and lacks sharpness, while a score of 5
means it provides perfect focus and
sharpness as a high-quality portrait.
4. Artifacts. Please score the extent of
artifacts in this picture. The score range is
1-5. A score of 1 means the picture has
unbearable amount of artifacts, while a score
of 5 means the picture is almost artifact-
free.
5. Texture. Please score the extent that the
picture correctly exhibits the texture of the
skin. A score of 1 means the skin in the
picture looks extremely different from real
humans, while a score of 5 means the skin in
the picture looks very genuine.

Please evaluate the provided picture and return
```

```
the score to me in the following format:
'''
Reality: []; Alignment: []; Focus and Sharpness:
[]; Artifacts: []; Texture: [].
You should strictly follow the above format and
put your actual evaluation score based on the
above criteria into each '[]'. Note this is
very important to my career. You should be as
fair as possible.
```

C. Additional Results

C.1. Editing

Our AGT-DM has the capability to perform texture editing through text prompts. To facilitate editing in our AGT-DM, we set lower values ($\omega_p = 0.01, \omega_e = 0.005$) to our photometric and edge guidance scalars to loosen the guidance controls and enable more effective editing. The editing results, shown in Fig. 11, illustrate the efficacy.

C.2. Out-of-Domain Generation

UltrAvatar is capable of producing high-quality fictional characters, comic figures and diverse out-of-domain characters. The results, shown in Fig. 12, illustrate the high quality, extensive diversity and excellent fidelity of our UltrAvatar generation.

C.3. Animation

We show five animated video sequences to demonstrate the animatability of generated avatars. From two source videos, we extract the motion parameters (expression codes and pose codes) from EMOCA, and then apply these to animate our generated avatars. Each animations is rendered from two different viewpoints under a specific lighting condition.

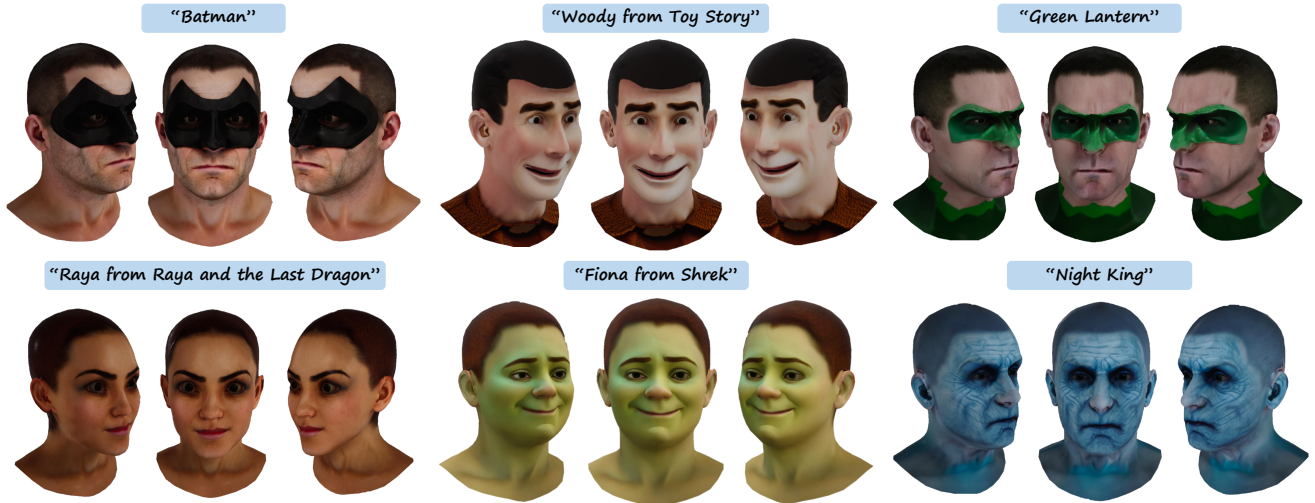


Figure 12. **Out-of-Domain Generation.** UltraAvatar is able to generate high-quality fictional Characters, comic figures and diverse out-of-domain characters.

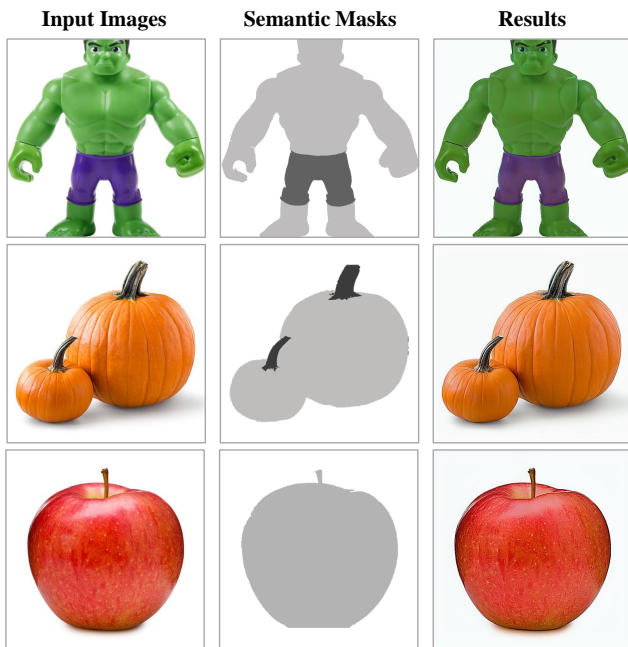


Figure 13. **DCE Results.** The results indicate that our DCE model is effective in removing specular highlights and shadows.

C.4. Ablation

DCE Model. We show more diffuse color extraction results in the Fig. 13. We select three images of different objects with specular highlights and shadows, and create semantic masks as input for our DCE model, the results provide a better demonstration of the efficiency and accuracy of our DCE model in handling a range of lighting removal tasks.

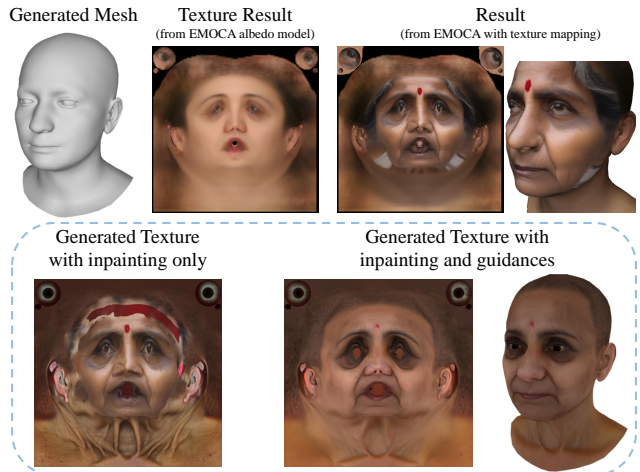


Figure 14. **Comparison with EMOCA and Texture Inpainting (w/o authenticity guidance).** EMOCA and texture inpainting produce textures with misalignment between the texture and the mesh and inconsistency in the boundary areas.

AGT-DM. In our comparative analysis, we evaluate our method against EMOCA and the texture inpainting technique that does not incorporate authenticity guidance, shown in Fig. 14. Both EMOCA and the non-authenticity-guided texture inpainting tend to yield textures with inconsistencies, primarily suffering from issues of misalignment between the generated texture and mesh and mismatch between the visible and inpainted regions. Our AGT-DM excels in generating consistent textures while effectively eliminating misalignment between the mesh and the texture, thereby enhancing the overall coherence and quality of the output.